

Phase transition dynamics for hot nuclei

INDRA Collaboration

B. Borderie^a, N. Le Neindre^b, M. F. Rivet^{a,1}, P. Désesquelles^c, E. Bonnet^d,
 R. Bougault^b, A. Chbihi^e, D. Dell'Aquila^{a,f}, Q. Fable^e, J.D. Frankland^e,
 E. Galichet^{a,g}, D. Gruyer^b, D. Guinet^h, M. La Commara^f, I. Lombardoⁱ,
 O. Lopez^b, L. Manduci^{b,j}, P. Napolitani^a, M. Pârlog^{b,k}, E. Rosato^{f,1},
 R. Roy^l, P. St-Onge^{e,1}, G. Verdeⁱ, E. Vient^b, M. Vigilante^f, J.P. Wieleczko^e

^a*Institut de Physique Nucléaire, CNRS/IN2P3, Univ. Paris-Sud, Université Paris-Saclay, Orsay, France*

^b*LPC, CNRS/IN2P3, Ensicaen, Université de Caen, Caen, France*

^c*CSNSM, CNRS/IN2P3, Univ. Paris-Sud, Université Paris-Saclay, Orsay, France*

^d*SUBATECH, IMT Atlantique, Université de Nantes, CNRS-IN2P3, Nantes, France*

^e*GANIL, (CEA/DRF-CNRS/IN2P3), Caen, France*

^f*Dipartimento di Fisica 'E. Pancini' and Sezione INFN, Università di Napoli "Federico II", Napoli, Italy*

^g*Conservatoire National des Arts et Métiers, Paris, France*

^h*Institut de Physique Nucléaire, CNRS/IN2P3, Univ. Claude Bernard Lyon 1, Université de Lyon, Villeurbanne France*

ⁱ*INFN, Sezione di Catania, Catania, Italy*

^j*Ecole des Applications Militaires de l'Energie Atomique, Cherbourg, France*

^k*Hulubei National Institute for R & D in Physics and Nuclear Engineering (IFIN-HH), Bucharest-Măgurele, Romania*

^l*Université Laval, Québec, Canada*

Abstract

An abnormal production of events with almost equal-sized fragments was theoretically proposed as a signature of spinodal instabilities responsible for nuclear multifragmentation in the Fermi energy domain. On the other hand finite size effects are predicted to strongly reduce this abnormal production. High statistics quasifusion hot nuclei produced in central collisions between Xe and Sn isotopes at 32 and 45 A MeV incident energies have been used to definitively establish, through the experimental measurement of charge correlations, the presence of spinodal instabilities. N/Z influence was also

¹deceased

studied.

Keywords: Quasifusion reactions, nuclear multifragmentation, spinodal instabilities, phase transition dynamics, N/Z effects

During the last decades the thermodynamics of finite nuclear systems was widely studied with heavy-ion collisions at intermediate and relativistic energies and with hadron-nucleus collisions at relativistic energies [1, 2]. With such collisions, depending on impact parameter, a nuclear system can be heated, compressed and then diluted. These systems are expected to undergo a liquid-gas type phase transition that manifests itself through nuclear multifragmentation [3]. This theoretical expectation, discussed for many years for nuclear matter [4, 5, 6, 7] is due to the similarity between the nuclear interaction and the Van der Waals forces acting in classical fluids [6, 8]. However, a nucleus (or a nuclear system) is a finite system which shows specific behaviours in the transition region. Most of the predicted specific signals of phase transition are a direct consequence of the local convexity of the entropy which is expected for finite systems having a discontinuous transition in the thermodynamic limit [9, 10, 11, 1]. By considering the microcanonical ensemble with energy as extensive variable, the convex intruder implies a backbending in the temperature (first derivative of entropy) at constant pressure and correlatively a negative branch for the heat capacity (second derivative). Experimentally, these two converging signatures have been observed from very different analyses. Negative heat capacities with a microcanonical sampling, were observed for 35 A MeV Au+Au semi-peripheral collisions [12] and confirmed by the INDRA collaboration for 32-50 A MeV Xe+Sn central collisions [8]. For caloric curves, their shape depends on the path followed by the system on the microcanonical equation of state surface, and a backbending (direct signature) can only be observed for a transition at constant pressure [13]. This was evidenced very recently for central 32-50 A MeV Xe+Sn collisions, thanks to a simulation based on experimental data [14] where a quantal temperature was calculated from the momentum fluctuations of protons present at freeze-out [15]. Pressure and volume-constrained caloric curves could be built and the expected behaviours were observed: a backbending for selected ranges of pressure and a monotonous increase at constant average volume [16]. Another consequence of the entropy curvature anomaly manifests itself when systems are treated in the canonical ensemble. In this case a direct phase transition signature is the presence of a bimodal

distribution of an order parameter [17] like the charge (size) of the largest fragment (Z_{max}) of multifragmentation partitions. Bimodality was observed (with a canonical sampling) in 60-100 A MeV Au+Au semi-peripheral collisions, allowing moreover to estimate the latent heat for nuclei close to gold around 8 MeV per nucleon and to set the appearance of the pure gas phase above 9-10 MeV per nucleon excitation energy [18].

The answer to a key point was still pending: it concerns the nature of the dynamics of the transition, i.e. fragment formation. Two mechanisms have been proposed. On one side, stochastic mean field approaches predict the fragmentation process to follow the spinodal fragmentation scenario triggered by phase-space fluctuations amplified in an unstable medium and, on the other side, in molecular dynamics models (QMD, AMD) many-body correlations are sufficient to produce fragments at early times even in absence of unstable conditions [10, 19, 20, 21, 22, 23, 24]. Experimentally, there was an indication that multifragmentation may be induced by spinodal instabilities but the confidence level of the fossil signature was not sufficient (3-4 σ), due to low statistics, to allow drawing any definitive conclusion [25, 26, 27]. Such instabilities may occur when the system evolves through the mechanically unstable spinodal region of the phase diagram, located at densities $\rho \leq \rho_0$ and temperatures below the critical temperature. Such conditions are well explored in central nuclear collisions around Fermi energy [28]. Moreover, if spinodal instabilities are at the origin of fragmentation, a reduction of instabilities for N/Z asymmetric systems in relation with an increase of the instability growth time is theoretically predicted [29]. In this letter we shall describe studies obtained with very high statistics (a factor 10 to 15 higher as compared to previous experiments) aiming to give a final answer as far as spinodal fragmentation is concerned and, secondly, to search for the related isospin effects.

The experiment was performed at GANIL (Grand Accélérateur National d'Ions Lourds) and two reactions were used $^{124,136}\text{Xe}+^{112,124}\text{Sn}$ at two bombarding energies, 32 and 45 A MeV, The beam, impinging on thin targets ($530\mu\text{g cm}^{-2}$), had an intensity of about 3-5 10^7 ions per second to avoid event pile-up. Experimental data were collected with the 4π multidetector INDRA which is described in detail in Refs. [30, 31]. Accurate particle and fragment identifications were achieved and the energy of the detected products was measured with an accuracy of 4%. Further details can be found in Refs. [32, 33, 34].

The data used in the analysis were obtained with an on-line multiplic-

ity trigger of 4 or more detected reaction products. The number of such recorded events was between 60 and 80 million events for each colliding system. Quasi-complete events are selected by requiring that at least 80% of the total charge of the system is measured. We then isolate compact shape events (quasifusion) through the additional condition that the flow angle (θ_{flow}) be larger than 60° . Let us recall that θ_{flow} characterizes the main direction of matter emission in the center of mass of the reaction and is determined by the kinetic energy flow tensor calculated from fragments ($Z \geq 5$) [35]. Measured cross-sections corresponding to selected events are ≈ 40 mb at 32 A MeV and 25 mb at 45 A MeV. They were derived from the measured target thicknesses, the counting of ions collected in the Faraday cup located at the end of the beam line and the acquisition dead time. The charge of ions reaching the cup was obtained using the formulas of Ref. [36]. Total cross-sections for quasifusion events, taking into account detection efficiency and selection biases, are estimated to be ~ 250 mb at 32 A MeV, and ~ 180 mb at 45 A MeV.

In infinite nuclear matter the signature of spinodal instabilities is the formation of equal-sized fragments due to density fluctuations which grow exponentially with time. The most unstable modes correspond to wavelengths lying around $\lambda \approx 10$ fm and the associated characteristic times are equal to around 30-50 fm/c, depending on density ($\rho_0/2 - \rho_0/8$) and temperature (0-9 MeV) [37, 38]. A direct consequence of the dispersion relation is the production of “primitive” fragments with size $\lambda/2 \approx 5$ fm which correspond to $Z \approx 8 - 10$. However, this simple picture is expected to be largely blurred by several effects. The beating of different modes occurs. Coalescence effects due to the nuclear interaction between fragments before the complete disassembly are also expected. For finite systems the situation is even more complicated. The presence of a surface introduces an explicit breaking of the translational symmetry with the important result that the growth rates are nearly the same for different multipolarities, which indicates that the unstable finite system breaks into different channels depending on multipolarity L [39]. Equal-sized “primitive” fragments are then expected to be produced with sizes in the range $A_F/2 - A_F/L_{max}$; A_F being the part of the system leading to fragments during the spinodal fragmentation. Moreover the finite system produced during the nucleus-nucleus collision has to stay or live long enough in the spinodal region (~ 3 characteristic time -100-150 fm/c - for symmetric matter) to allow an important amplification of the initial density fluctuations. And finally, we experimentally detect fragments after secondary decay, which introduces a broadening of the fragment size dis-

tribution. Taking into account the accumulation of all these effects on the final extra production of equal-sized fragments, it is clear that any signature that spinodal fragmentation is responsible for the phase transition dynamics can only be what we have called a fossil signature. A full simulation of the spinodal decomposition of quasifused sources using Brownian One-Body dynamics calculations [26] already testified to this fact, with less than 1% of events with equal-sized fragments. It is the reason why the signature is difficult to observe experimentally.

Twenty years ago an intra-event correlation function called higher order charge correlations [40] was proposed to enlighten any extra production of events with specific fragment partitions. The high sensitivity of the method makes it particularly appropriate to look for small numbers of events as those expected to have kept a memory of spinodal fragmentation properties.

All fragments of one event with fragment multiplicity $M = \sum_Z n_Z$, where n_Z is the number of fragments with charge Z in the partition, are taken into account. By means of the normalized first order:

$$\langle Z \rangle = \frac{1}{M} \sum_Z n_Z Z \quad (1)$$

and second order:

$$\sigma_Z^2 = \frac{1}{M} \sum_Z n_Z (Z - \langle Z \rangle)^2 \quad (2)$$

moments of the fragment charge distribution in the event, one may define the correlation function (CF):

$$1 + R(\sigma_Z, \langle Z \rangle) = \frac{Y(\sigma_Z, \langle Z \rangle)}{Y'(\sigma_Z, \langle Z \rangle)} \Big|_M \quad (3)$$

Here, the numerator $Y(\sigma_Z, \langle Z \rangle)$ is the yield of events with given $\langle Z \rangle$ and σ_Z values. Because the measurement of the charge belonging to a given event is not subject to statistical fluctuations, we use here expression (2) rather than the “nonbiased estimator” of the variance, $\frac{1}{M-1} \sum_Z n_Z (Z - \langle Z \rangle)^2$, as proposed in [40]. The denominator $Y'(\sigma_Z, \langle Z \rangle)$ represents the uncorrelated yield. Its retained evaluation is based on the “intrinsic probability”, ${}^{\text{intr}}P_Z$, of emission of a given charge. A unique set of intrinsic probabilities exists only if the chosen event sample is extracted from single-source events. The denominator partition probabilities are built to take into account in a combinatorial way the trivial correlations due to charge conservation. Thus, this

denominator replicates all features of the partitions of the numerator, except the correlations due to other reasons than charge conservation. The probability to observe a given partition ($\mathbf{n} : (n_1, \dots, n_{Z_{\max}})$), at a given total multiplicity, $m = \sum_Z n_Z$, is obtained by the multinomial formula. If the total charge is fixed ($Z_{\text{tot}} = \sum_Z Z n_Z$), the partition probabilities are given by:

$$P(\mathbf{n}|m) = \alpha m! \prod_Z \frac{{}^{\text{intr}}P_Z^{n_Z}}{n_Z!} \delta_{Z_{\text{tot}}, \sum_Z Z n_Z} , \quad (4)$$

where α is the normalization constant (so that $\sum_n P(\mathbf{n}|m) = 1$) and δ is the Kronecker symbol. All the details can be found in Refs. [26, 41]. The ${}^{\text{intr}}P_Z$ values are obtained by means of a recursive procedure of minimization which stops when the decreasing between two steps is lower than 10^{-12} . The minimization criterion is the normalized χ^2 between the experimental partition probabilities and the calculated partition probabilities for a considered set of data. The calculated χ^2/N_{dof} were always in the range 1.0-0.7: the lower is the incident energy and the larger is the multiplicity, the lower is the χ^2 value. Fig. 1 shows one example on how the experimental charge distributions are faithfully described. The intrinsic probabilities, ${}^{\text{intr}}P_Z$, have been calculated independently for each incident energy, for each reaction and for the different fragment multiplicities. Finally, to evaluate the sensitivity of the intrinsic probability method for measuring CFs, we have performed a Monte-Carlo simulation. The created events obey the following conditions: as for data, events are selected by requiring at least 80% of the charge of a system with $Z=104$, charged reaction products are produced according to the probability $P(Z) \propto \exp(-0.1Z)$ and fragments have $Z \geq 5$. M was chosen equal to 4. As expected, CF values are close to one everywhere and, for low σ_Z (<2), calculated CF values are in the range 0.95-1.05; this last value determines the limit of sensitivity.

We shall present now the CF results for the considered samples of events i.e. those with 3 to 6 fragments ($Z \geq 5$) which correspond to higher statistics. First of all, we must define what is the optimum variance bin σ_Z bearing in mind that emitted primary fragments in these reactions have excitation energies of around 3 MeV per nucleon [42, 14]. Fig. 2 illustrates the CF measured for the different fragment multiplicities with bins equal to one in $\langle Z \rangle$ and σ_Z . It concerns single source events selected at 32 A MeV for the ${}^{124}\text{Xe}+{}^{112}\text{Sn}$ reaction. For clarity of presentation, when the statistical error of the numerator, $Y(\sigma_Z, \langle Z \rangle)$, was greater than or equal to 50%, CF value

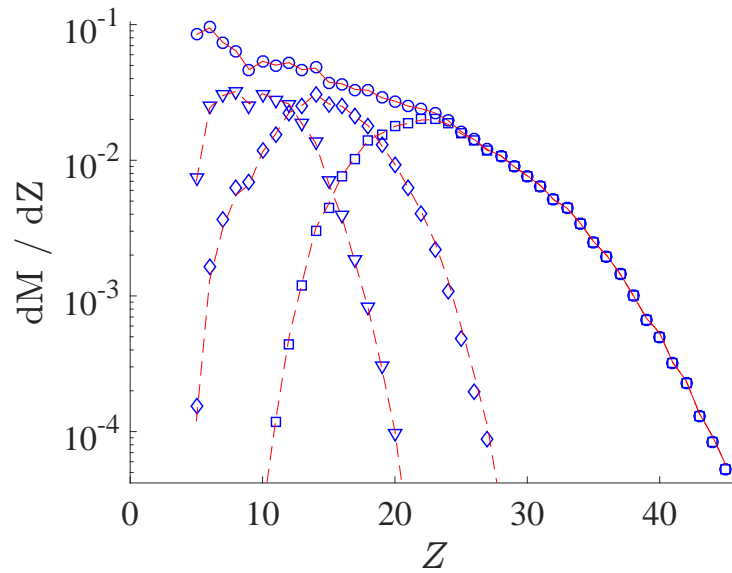


Figure 1: (Color online) Experimental differential charge multiplicity distribution (circles) for the single source formed in central 32 A MeV $^{124}\text{Xe}+^{112}\text{Sn}$ reaction with fragment multiplicity equal to 4. Experimental differential distributions for the first (squares), second (diamond) and third (triangles) heaviest fragments of partitions are presented too. The full and dashed lines, to be compared to data, correspond to the results of the intrinsic probability method for the fragment probabilities.

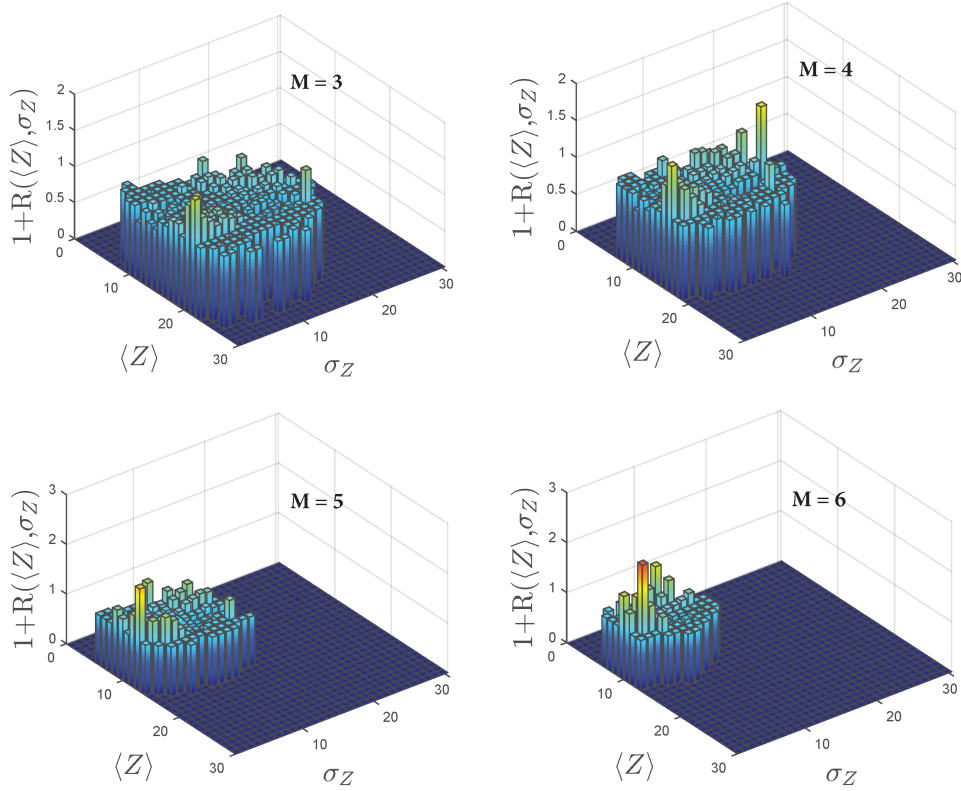


Figure 2: (Color online) Experimental correlation functions for selected quasifusion events formed in central 32 A MeV $^{124}\text{Xe}+^{112}\text{Sn}$ collisions, for fragment multiplicities 3 to 6. The color/gray scale is the same for all figures and the maximum value of 3 for correlation functions corresponds to dark red/dark gray.

was fixed to one. We observe significant peaks (CF values in the range 1.4 - 2.1) for $\sigma_Z < 1$ for each fragment multiplicity. For the first time, the limited ranges of $\langle Z \rangle$ contributing to CF peaks are clearly observed (see also Table 1), which verify what is expected for finite systems i.e. $M \times \langle Z \rangle \sim \text{constant}$. We can then build CFs for all events, whatever their multiplicity, by summing the correlated yields of all M and by replacing the variable $\langle Z \rangle$ by $M \times \langle Z \rangle$. Uncorrelated yields are constructed and weighted in proportion to real events of each multiplicity. In Fig. 3 the resulting CF is displayed; the $M \times \langle Z \rangle$ bin is now equal to three. As for Fig. 2 CFs have been fixed to one when the statistical error on the correlated yield was

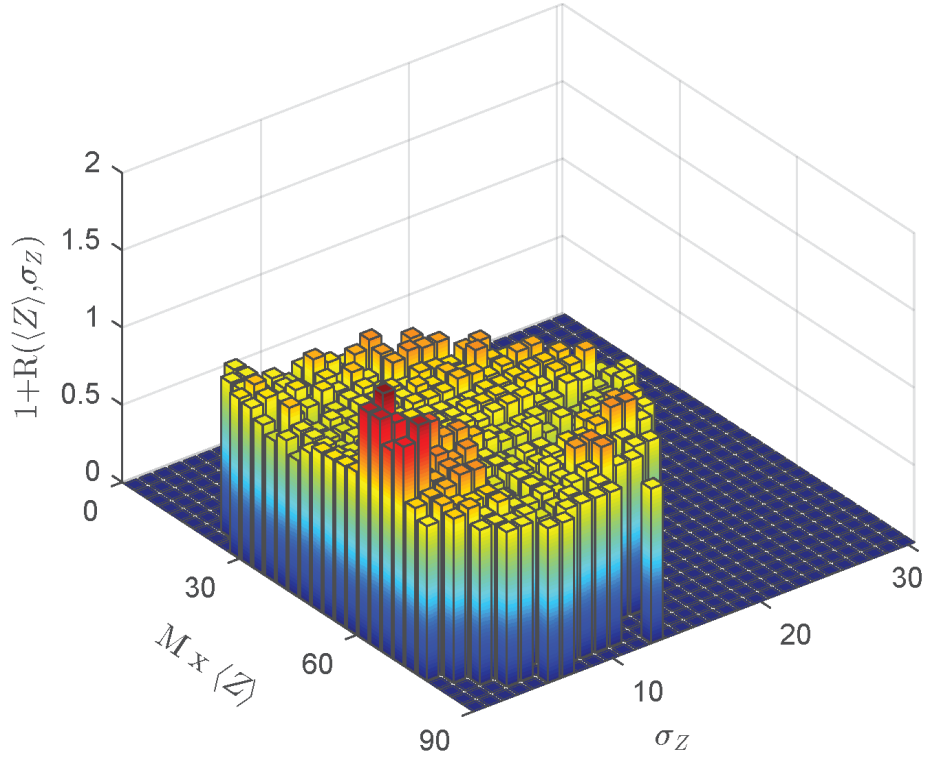


Figure 3: (Color online) Experimental correlation function for selected quasifusion events formed in central 32 A MeV $^{124}\text{Xe}+^{112}\text{Sn}$ collisions. Events with fragment multiplicities 3 to 6 are mixed. Correlation function is calculated for a σ_Z bin equal to 1 and a $M \times \langle Z \rangle$ bin equal to 3. The color/gray scale for CFs has a maximum value for 1.6 which corresponds to dark red/dark gray.

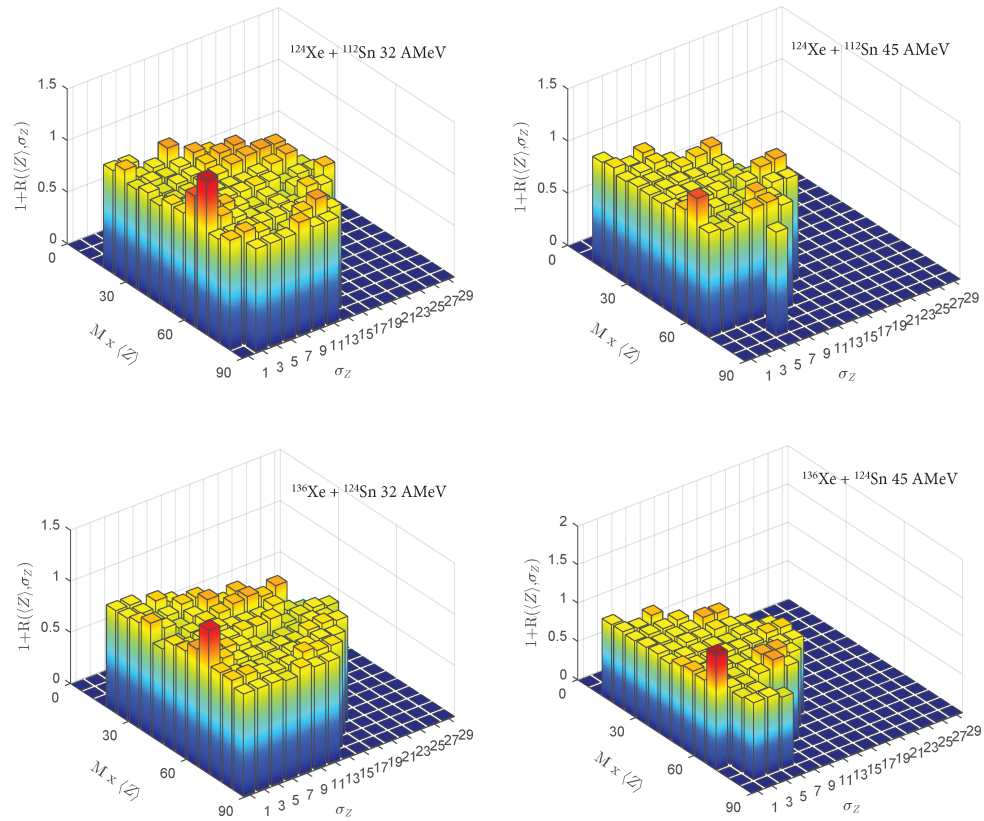


Figure 4: (Color online) Experimental correlation functions for selected quasifusion events formed in central $^{124,136}\text{Xe} + ^{112,124}\text{Sn}$ collisions. Events with fragment multiplicities 3 to 6 are mixed. Correlation functions are calculated for a σ_Z bin equal to 2 and a $M \times \langle Z \rangle$ bin equal to 6. The color/gray scale for CFs has a maximum value for 1.6 which corresponds to dark red/dark gray.

Table 1: Characteristics of events with $\sigma_Z < 2$ for the different incident energies and reactions. For each fragment multiplicity M , the range of $\langle Z \rangle$ contributing to the correlation peaks are indicated; $\langle Z \rangle$ within parentheses have CF values lower or equal to 1.1.

M		3	4	5	6
E (AMeV)	reaction				
32	$^{124}\text{Xe}+^{112}\text{Sn}$	20 - 22	15 - 18	12 - 14	10 - 12
32	$^{136}\text{Xe}+^{124}\text{Sn}$	20 - 22	15 - 18	12 - 15	10 - 12
45	$^{124}\text{Xe}+^{112}\text{Sn}$	18 - 20	14 - 16	10 - 12	8 - 10
45	$^{136}\text{Xe}+^{124}\text{Sn}$	(16 - 20)	(12 - 16)	(10 - 14)	(8-10) - 12

equal or greater than 50%. As expected a limited region with CF values greater than one (1.34 - 1.49) is observed at very low $\sigma_Z (< 1)$ for $M \times \langle Z \rangle$ bins 60-63, 63-66, 66-69 and 69-72. We also highlight with the help of the present figure a complementary contribution coming from σ_Z (1 - 2) with CF values (1.31 - 1.57) equivalent to the previous ones that one must take into account. This fixes the upper limit at 2 for the σ_Z of events with nearly equal-sized fragments. The complementary contribution comes from the broadening of the fragment Z distribution introduced by the deexcitation of primitive fragments. On the observed Z range for fragments, simulations of their deexcitation from 3 MeV per nucleon excitation energy [42, 14] generate an extra σ_Z value of around one unit [43, 44]. Note that two other regions with CF values greater than one appear in the figure. A first one, at low $M \times \langle Z \rangle$ values, which corresponds to quasifusion-evaporation events with emission of several light fragments associated to the evaporation residues and a second, at high $M \times \langle Z \rangle$ values, coming from quasifusion-fission events accompanied by one or two light fragments. Fig. 4 (upper left) results from what we learned from Fig. 3 i.e. to use larger bins in both σ_Z (2 units) and $M \times \langle Z \rangle$ (6 units). We observe only two CF peak at low σ_Z with values 1.27 and 1.50 which cover the $M \times \langle Z \rangle$ range 60-72. Their confidence levels in sigma units, obtained from the deviation to 1, $R(\sigma_Z, \langle Z \rangle)$, of the correlation function, normalized to its statistical error bar, $\sigma_{1+R(\sigma_Z, \langle Z \rangle)}$, calculated from the numerator only are respectively equal to 6.09 and 7.29, which definitively establishes the presence of spinodal fluctuations.

The procedure described above was followed for the three other studied systems. We see in Table 1 that, whatever the incident energy and the

Table 2: CF peaks with $\sigma_Z < 2$: values and confidence levels for the different incident energies and reactions.

E (AMeV)	reaction	$M \times \langle Z \rangle$ range	CF value	conf. level (sigma units)
32	$^{124}\text{Xe} + ^{112}\text{Sn}$	60-66	1.268	6.09
		66-72	1.498	7.29
32	$^{136}\text{Xe} + ^{124}\text{Sn}$	60-66	1.143	2.98
		66-72	1.402	6.47
45	$^{124}\text{Xe} + ^{112}\text{Sn}$	54-60	1.075	2.29
		60-66	1.257	0.82
45	$^{136}\text{Xe} + ^{124}\text{Sn}$	66-72	1.502	2.08

reaction, the same or very similar $\langle Z \rangle$ ranges are contributing to the correlation peaks for the two reactions. We also note that, except for the highest multiplicity, low CF values were measured for the neutron rich system at 45 A MeV incident energy, which makes more difficult a precise determination of the $\langle Z \rangle$ range. Fig. 4 summarizes the results. As for Figs. 2 and 3, CFs have been fixed to one when the statistical error on the correlated yield was equal or greater than 50%. For the four systems we observe CF peaks at low σ_Z with values varying from 1.08 to 1.50 and confidence levels from 0.82 to 7.29 sigma units (see also Table 2). Covered $M \times \langle Z \rangle$ domains are the same (60 - 72) for both reactions at 32 A MeV incident energy whereas at higher incident energy the neutron rich system covers a range a little bit higher (66 - 72) than the neutron poor one (54 - 66). Finally the percentages of events ($Y(\sigma_Z, \langle Z \rangle)$ /total number of events) and extra events ($Y(\sigma_Z, \langle Z \rangle) - Y'(\sigma_Z, \langle Z \rangle)$) measured are reported in Table 3. Within error bars, extra event percentages are similar for both systems at the lower incident energy. At higher incident energy we observe a strong reduction of percentages, in particular for the neutron rich system. The observation of the reduction with incident energy, at least for the more symmetric system, is in good agreement with the negative heat capacity signatures observed experimentally which fixed the upper limit of the coexistence zone (spinodal region) in the incident energy range 39-50 A MeV [8]. This coherence between both signals was not clearly observed from previous charge correlation studies [26, 2]. The large reduction of the signal observed for the neutron rich

Table 3: Numbers and percentages of events and extra events with $\sigma_Z < 2$ for the different incident energies and reactions. Calculated errors are statistical.

E (AMeV)	reaction	events	(%)	extra events	(%)
32	$^{124}\text{Xe}+^{112}\text{Sn}$	1313	0.27	336	0.068 ± 0.004
32	$^{136}\text{Xe}+^{124}\text{Sn}$	1077	0.32	217	0.064 ± 0.004
45	$^{124}\text{Xe}+^{112}\text{Sn}$	1073	0.34	77	0.025 ± 0.003
45	$^{136}\text{Xe}+^{124}\text{Sn}$	68	0.030	15	0.0065 ± 0.0017

system, a factor ten between 32 and 45 A MeV, can be understood in terms of the expected N/Z influence. Indeed, if spinodal instabilities are at the origin of the dynamics of multifragmentation, as discussed before, theoretical calculations predict a reduction of instabilities for asymmetric systems in relation with an increase of the instability growth time. More precisely, it is shown in [29] that, for *Sn* isotopes, the most unstable modes associated to shorter instability growth times ($\simeq 50$ fm/c) disappear when N/Z changes from 1.40 to 1.64. If we consider that quasifusion systems produced by the collisions, with N/Z varying from 1.27 to 1.50, have to stay long enough in the spinodal region (~ 3 characteristic times) to allow important amplification of the initial fluctuations, one can qualitatively understand the large extra reduction of the correlation signal for the neutron rich system at high incident energy as coming from insufficient reaction time. Such a situation also favors coalescence of primary fragments. Finally, note that the set of reaction trajectories in the density - temperature plane, close to the border of the spinodal region at 45 A MeV can be slightly different for the two reactions.

In conclusion, two reactions $^{124}\text{Xe}+^{112}\text{Sn}$ and $^{136}\text{Xe}+^{124}\text{Sn}$ have been used at two bombarding energies, 32 and 45 A MeV, to produce quasifusion hot nuclei which undergo multifragmentation. Using charge correlations the fossil signature of spinodal instabilities i.e. the abnormal presence of equal-sized fragments was definitively established at a confidence level of around 6 - 7 sigma units for both reactions at 32 A MeV incident energy. At higher bombarding energy we observe a reduction of the signal (by a factor around 3) for the more symmetric system. This reduction is in good agreement with the negative heat capacity signature previously observed which fixed the upper limit of the spinodal region in the incident energy range 39-50 A MeV.

The most important reduction of the signal is registered for the neutron rich system (a factor around 10 between 32 and 45 A MeV incident energies). This observation is consistent with the theoretical expectation of an increase of the instability growth time of spinodal fluctuations with an increase of N/Z for the hot nuclei.

The nature of the dynamics of the transition, i.e. the fragment formation was the last missing piece of the puzzle concerning the first order phase transition for hot nuclei. At this point one can emphasize that multifragmentation was early theoretically associated to a phase transition for nuclear matter. Then multifragmentation became a generic term to name a reaction where several fragments were observed in the exit channel. From the present knowledge one can infer that the generic term covers at least the reaction mechanisms involved in the phase transition region and in the vaporization regime. We recall that one can locate the onset of a pure gas phase at a thermal excitation energy of around 9-10 MeV per nucleon [45, 18, 16]. It should be also pointed out that, beyond the fragment production which we can connect to spinodal instabilities and vaporization, the fragmentation process may also arise from other dynamics like cavitation and nucleation.

Acknowledgements

One of the authors B.B. want to underline the major role played by theoreticians of this domain during the last twenty years of the previous century to give some guidance to experimentalists equipped with powerful multidetectors.

References

- [1] P. Chomaz et al. (eds.), Dynamics and Thermodynamics with Nuclear Degrees of Freedom, Eur. Phys. J. A 30 (2006) and references therein.
- [2] B. Borderie, M.F. Rivet, Prog. Part. Nucl. Phys. 61 (2008) 551 and references therein.
- [3] J. P. Bondorf et al., Phys. Lett. B 162 (1985) 30.
- [4] H. Schulz et al., Phys. Lett. B 119 (1982) 12.
- [5] M. W. Curtin et al., Phys. Lett. B 123 (1983) 219.
- [6] H. R. Jaqaman et al., Phys. Rev. C 27 (1983) 2782.

- [7] H. Müller, B. D Serot, Phys. Rev. C 52 (1995) 2072.
- [8] B. Borderie, J. Phys. G: Nucl. Part. Phys. 28 (2002) R217.
- [9] D.J. Wales and R. S. Berry, Phys. Rev. Lett. 73 (1994) 2875.
- [10] P. Chomaz, M. Colonna and J. Randrup, Phys. Rep. 389 (2004) 263.
- [11] F. Gulminelli, Ann. Phys. Fr. 29 6 (2004).
- [12] M. D'Agostino et al., Phys. Lett. B 473 (2000) 219.
- [13] P. Chomaz, V. Duflot and F. Gulminelli, Phys. Rev. Lett. 85 (2000) 3587.
- [14] S. Piantelli et al., INDRA Collaboration, Nucl. Phys. A 809 (2008) 111.
- [15] H. Zheng and A. Bonasera, Phys. Lett. B 696 (2011) 178.
- [16] B. Borderie et al. INDRA Collaboration, Phys. Lett. B 723 (2013) 140.
- [17] P. Chomaz, F. Gulminelli and V. Duflot, Phys. Rev. E 64 (2001) 046114.
- [18] E. Bonnet et al., INDRA Collaboration, Phys. Rev. Lett. 103 (2009) 072701.
- [19] C. Hartnak et al., Eur. Phys. J. A 1 (1998) 151.
- [20] R. Neubauer et al., INDRA Collaboration, Nucl. Phys. A 658 (1999) 67.
- [21] A. Ono, Phys. Rev. C 59 (1999) 853.
- [22] A. Ono et al., Phys. Rev. C 66 (2002) 014603.
- [23] J.D. Frankland et al., INDRA Collaboration, Nucl. Phys. A 689 (2001) 940.
- [24] J. Rizzo et al., Phys. Rev. C 76 (2007) 024611.
- [25] B. Borderie et al. INDRA Collaboration, Phys. Rev. Lett. 86 (2001) 3252.
- [26] G. Tăbăcaru et al., Eur. Phys. J. A 18 (2003) 103.

- [27] B. Borderie and P. Désesquelles, *Eur. Phys. J. A* 30 (2006) 243.
- [28] E. Bonnet et al., *Phys. Rev. C* 89 (2014) 034608.
- [29] M. Colonna, P. Chomaz and S. Ayik, *Phys. Rev. Lett.* 88 (2002) 122701.
- [30] J. Pouthas et al., *Nucl. Instr. and Meth. in Phys. Res. A* 357 (1995) 418.
- [31] J. Pouthas et al., *Nucl. Instr. and Meth. in Phys. Res. A* 369 (1996) 222.
- [32] G. Tăbăcaru et al., INDRA Collaboration, *Nucl. Instr. and Meth. in Phys. Res. A* 428 (1999) 379.
- [33] M. Pârlog et al., INDRA Collaboration, *Nucl. Instr. and Meth. in Phys. Res. A* 482 (2002) 674.
- [34] M. Pârlog et al., INDRA Collaboration, *Nucl. Instr. and Meth. in Phys. Res. A* 482 (2002) 693.
- [35] J.D. Frankland et al., INDRA Collaboration, *Nucl. Phys. A* 689 (2001) 905.
- [36] G. Schiwietz and P. L. Grande, *Nucl. Instr. and Meth. B* 175 (2001) 125.
- [37] M. Colonna, P. Chomaz and A. Guarnera., *Nucl. Phys. A* 613 (1997) 165.
- [38] P. Napolitani and M. Colonna, *Phys. Rev. C* 96 (2017) 054609.
- [39] B. Jacquot et al., *Phys. Lett. B* 383 (1996) 247.
- [40] L. G. Moretto et al., *Phys. Rev. Lett.* 77 (1996) 2634.
- [41] P. Désesquelles, *Phys. Rev. C* 65 (2002) 034604.
- [42] S. Hudan et al., INDRA Collaboration, *Phys. Rev. C* 67 (2003) 064613.
- [43] D. Durand, *Nucl. Phys. A* 541 (1992) 266.
- [44] R.J. Charity, *Phys. Rev. C* 82 (2010) 014610.
- [45] J. Pochodzalla et al., ALADIN Collaboration, *Phys. Rev. Lett.* 75 (1995) 1040.